Validations of satellite ozone profiles in austral spring using ozonesonde measurements in the Jang Bogo station, Antarctica

Hana Lee[1], Taejin Choi[2], Seong-Joong Kim[2], Juseon Bak[3], Dha Hyun Ahn[1], Natalya Alekseyevna Kramarova[4], Sang Seo Park[5], Jhoon Kim[1], and Ja-Ho Koo[1,*]

[1]Department of Atmospheric Sciences, Yonsei University, Seoul, South Korea

[2]Korea Polar Research Institute, Incheon, South Korea

[3]Pusan National University, Busan, Korea

[4]NASA Goddard Space Flight Center, Greenbelt, MD, USA

[5]Ulsan National Institute of Science and Technology, Ulsan, South Korea

*** Corresponding Author:**

Ja-Ho Koo, Department of Atmospheric Sciences, Yonsei University, Seoul, Republic of Korea, E-mail: zach45@yonsei.ac.kr

Abstract

Using ozonesonde measurements from 2015 to 2018 at the Jang Bogo station located in the Antarctic region, we evaluate ozone profile retrieved from the three satellite measurements that are widely used: Ozone Monitoring Instrument (OMI), Microwave Limb Sounder (MLS), and Ozone Mapping Profiler Suite (OMPS) data. For the fair validation, ozonesonde profiles become smoothed using the a priori ozone profile used in the satellite retrieval algorithm (i.e., convolution process). Compared with limb-viewing MLS and OMPS ozone profiles, the OMI ozone profiles are relatively less qualified: coarser vertical resolution and larger inter-annual variation. Nevertheless, our validation reveals that the quality of all three satellite ozone profiles looks comparable; In general, difference from ozonesonde profile is ~1 ppm absolutely, and -20 to 30 % relatively at maximum. This quantitative range well corresponds to previous work, meaning that our new validation confirms the reliability of satellite ozone profiles in the Antarctic region once more. Another interesting feature is the role of a priori ozone profile. Despite the technical difficulty, nadir-viewing OMI satellite can have qualified ozone profiles by a proper assumption of a priori ozone profile. We think that the simultaneous usage of multiple satellite ozone profiles can contribute to better understanding of Antarctic ozone characteristics.

Keywords: Jang Bogo Station, ozonesonde, ozone profile, OMI, MLS, OMPS

1. Introduction

Since the stratospheric ozone hole in the Antarctic spring was officially reported in the early 1980s (Farman et al., 1985), ground-based and space-borne monitoring networks have been extensively established to understand the physicochemical process of atmospheric ozone. The Antarctic ozone hole issue prompted a worldwide phaseout of the production of anthropogenic halocarbons containing chlorine and bromine, which are known to be the primary sources of reactive halogens responsible for ozone depletion (WMO, 2014). Based on this scientific evidence, the Montreal Protocol, a global agreement to reduce human emissions of ozone-depleting gases, was started in 1987. Through effort in this action, the signs of ozone recovery have been reported since 2000. Solomon et al. (2016) showed the increases in the total ozone column (TOC) and changes in the vertical profile of ozone concentration over the Antarctic region. Goutail et al. (2018) also represented the large decrease of ozone hole area over the Southern Hemisphere. However, stratospheric ozone recovery is not perfectly guaranteed yet. Continuous ozone loss is especially detected in the upper troposphere and lower stratosphere (UTLS) of equatorial and mid-latitudinal regions (Ball et al., 2018; Ball et al., 2019).

This inconsistent trend of stratospheric ozone according to the altitude implies that the analysis of the ozone profile is an essential task for the accurate diagnosis of ozone depletion and its effect to the climate change. The balloon-borne ozonesonde is the representative method for in-situ monitoring of ozone profiles from the surface to ~ 35 km (Komhyr, 1986) and has been utilized as a standard dataset for examining the vertical structure of ozone. Although there are globally ~50 stations to conduct the routine measurement of ozonesonde, observations in the Antarctic region were quite limited. Ozonesonde observations in the southeastern Antarctic area were particularly rare, only a few at the McMurdo (Rabier et al., 2013; Gazeaux et al., 2013) and Bharati station (Hulswar et al., 2020). In this situation, the Korea Polar Research Institute (KOPRI) started the contribution to the Antarctic ozonesonde monitoring since 2014 at the Jang Bogo station located in the east Antarctic Ross Sea (Figure 1). Since the Brewer spectrophotometer (MK III, #220) has also monitored the total ozone (Kim

et al., 2021), the Jang Bogo station is the appropriate place for the inter-comparison of ozone profile from various techniques. This will be quite useful to evaluate the sensitivity of Antarctic air chemistry to the climate variability in different altitudes.

To get over the spatial limitation of ground-based monitoring, the satellite remote sensing has been also actively utilized for the Antarctic ozone monitoring. Instruments onboard the polar-orbit satellite can detect the atmospheric ozone, resulted in the retrieval of TOC and vertical ozone profiles. Two types of satellite measurements, nadir-viewing and limb-viewing, have been used for the ozone monitoring for a long time: e.g., the Ozone Monitoring Instrument (OMI) and the Microwave Limb Sounder (MLS) onboard the NASA Aura satellite. Wide spatial coverage of these satellite measurements enable us for the comprehensive investigation of the Antarctic ozone profile if they are qualified. Namely, the validation of satellite data quality is an essential step for accurate analysis of ozone pattern and relevant climate processes (Sepúlveda et al., 2021).

In this context, inter-comparison analyses have been significantly conducted between the ground-based and satellite ozone data. But these efforts were mostly for the validation of TOC measurement, not for that of ozone profile due to the deficiency of available in-situ ozone profiles. As a result, the accuracy of satellite TOC data has been well evaluated so far, but the quality of ozone profile from the satellite measurements is still remained uncertain. A few studies performed the validation of satellite ozone profile over the Antarctic region (e.g., Huang et al., 2017; Kramarova et al., 2018), but additional validations are much required to cover the whole Antarctic area. Most of the ground stations were installed in the western part of the Antarctic or in the coast of Antarctic, implying that the satellite measurements over the high latitude (> 70 ˚S) or over the eastern part of Antarctic were not much validated with the ground-based measurements.

As mentioned, the Jang Bogo station, the second Korean base in Antarctica, was installed in the high latitude of eastern Antarctic region (74.5 ˚S, 164.4 ˚E). Thus, ozonesonde observations here are

invaluable, enabling us to assess satellite ozone profile over the Antarctic region where the ground-based monitoring has not been performed much. In this study, we evaluate ozone profile products from several satellite measurements by comparing to the ozonesonde data at the Jang Bogo station, which resulted in a better understanding for the performance of satellite remote sensing for the ozone profile in eastern Antarctica. Section 2 describes the characteristic of ground-based and satellite ozone profile datasets, and Section 3 explains the validation methodology to compare satellite profiles with ozonesonde data. The results are presented and discussed in Section 4, and the summary of this study is presented in Section 5. We believe that all information in this study will suggest helpful ideas for the investigation of the ozone-climate connection in the Antarctic area.

2. Data

2.1 Ozonesonde observations

The ozonesonde is a well-established technique to observe the ozone profile from the surface to ~35 km with a vertical resolution of 100 to 150 m. It is equipped with a radiosonde, a global positioning system (GPS) receiver, and an electrochemical cell (ECC) sensor using an iodine-iodide redox method. The precision of ozonesonde is approximately 3–5%, and the accuracy is 5–10% (Komhyr, 1986; Komhyr et al., 1995; Anne et al., 2019). At the Jang Bogo station, ozonesondes (VAISALA GPS RS92G radiosonde and ECC) were usually launched in austral spring (from September to November) to monitor stratospheric ozone hole. Accordingly, vertical profiles of temperature, pressure, and ozone mixing ratio were collected. This study utilizes these ozonesonde data to evaluate ozone profiles from the satellite observation from 2015 to 2018. To avoid the inclusion of anomalous profiles, we screen out ozonesonde data if it bursts at a pressure exceeding 20 km or no measurement continues longer than 3 km vertically (Huang et al., 2017).

Owing to the wind influence, perpendicular observations of ozonesonde usually have the horizontal movements. Since the Jang Bogo station is the downwind area of the eastern Antarctic

plateau, which is strongly influenced by katabatic winds from the high-elevation (Yoo et al., 2018; Ahn et al. 2019), the launched ozonesonde is likely to drift eastward from the station while ascending. Figure 2 describes the horizontal trajectories of the ozonesonde in September, October, and November during 2015-2018. We calculate the distance range between the Jang Bogo station and the last location of the ozonesonde flight. As a result, the drift distance ranges is ~70.9 km at minimum (October 2015) and ~261 km at maximum (October 2017). The averaged distance between Jang Bogo station and ozonesonde flight is 158.6 km, latitude within ± 1.5˚, and longitude within ± 5˚ from Jang Bogo station. To utilize satellite data sufficiently for the comparison to the ozonesonde data, we designate the coincident criteria (i.e., spatial criteria of comparison), which is the latitude ± 3˚ and longitude ± 10˚. The detailed methodology is described in Section 3.

2.2 Satellite ozone profiles

In this study, our main objective is the evaluation of retrieved ozone profiles from the satellite remote sensing, which is composed of two different techniques, which are the nadir-viewing and limb-viewing satellite measurement; The limb-viewing instruments provide a higher vertical resolution (~ 3 km) but have limited spatial coverage and a coarse horizontal resolution than the nadir-viewing instruments. For this purpose, we use two nadir-viewing ozone profile products from OMI measurements and two limb-viewing ozone profile products from MLS and Ozone Mapping and Profiler Suite (OMPS) limb-profiler (LP) measurements. The general characteristics of these products are summarized in Table 1, and the vertical resolution of these data is depicted in Figure 3. Characteristics of these data in detail are described below.

2.2.1 OMI ozone profiles

The OMI is a nadir-viewing instrument onboard the Aura satellite. It uses the ultraviolet (UV) and visible (VIS) channels, measuring backscattered radiances in three bands in the wavelength range from

270 to 500 nm (UV-1: 270–310 nm, UV-2: 310–365 nm, VIS: 350–500 nm) with spectral resolutions of 0.42–0.63 nm (Levelt et al., 2018). A spatial resolution is 24 km × 13 km (across-track × along-track) at the nadir position for UV-2 and VIS channels, and 48km×13km for the UV-1 channel. Using these OMI measurements, ozone profiles can be retrieved from two algorithms named as OMO3PR and PROFOZ. For the retrieval, both OMO3PR and PROFOZ algorithms use the optimal estimation (OE) technique associated with the spectral range of 270-310 nm from the UV-1 channel and 310-330 nm from the UV-2 channel.

They have significantly different implementations in detail (Bak et al., 2015) as specified in Table 1. In both algorithms, two UV-2 spectra are co-added to match the UV-1 spatial resolution in the cross-track position. Due to the expensive computational budget, however, four along-track pixels are further co-added in the PROFOZ algorithm (spatial resolution is 48 × 52 km^2) while OMO3PR performs retrievals for one out of five UV-1 pixel along-track. Since nadir viewing instruments provide limited vertical information in the lower atmosphere, especially in high-latitudes due to the reduced photon penetration into the troposphere at high SZA, the OE technique combines a priori information with measurements to stabilize the retrieval. Both ozone profile products from the OMO3PR and PROFOZ algorithms use the climatological a priori information derived from Aura MLS and ozonesonde observations (McPeters et al., 2007). Relatively, the PROFOZ has been more extensively validated through long-term comparisons with multiple ozone data from satellite, ozonesonde, and ground-based observations, resulted in an overall agreement of 3–20 % (Huang et al., 2017; 2018). The best agreement was found between PROFOZ and Brewer spectrophotometer in the Arctic, which is a mean difference of within 1% at most (Bak et al., 2015). In January 2009, the occurrence of OMI row anomaly occurred, inducing some biases dependent on latitude, season, SZA, and cross-track positions (Huang et al., 2017).

For the comparison with ozonesonde in this study, we only use the level 2 ozone profiles of version 0.9.3 (Liu et al., 2010), which has been more frequently examined. The PROFOZ profiles of partial ozone columns are retrieved at 24 layers. We use a quality flag of a suitable pixel, according to van Oss

et al. (2002) and Liu et al. (2010).

2.2.2 MLS ozone profiles

The MLS is a limb-viewing instrument onboard the Aura satellite along with OMI. The MLS provides daily global coverage with ~15 orbits for the thermal emission measurement at 240 GHz microwave channel (Waters et al., 2006). We use the MLS version 4.2 Level-2 ozone profile product retrieved from the OE technique (Livesey et al., 2015) with a priori data taken from the climatology based on the model for ozone and related chemical tracers (MOZART). The a priori covariance is constructed using a considerable error value because the retrievals are not too sensitive to the values of the a priori (Lucien Froidevaux, personal communication). The MLS ozone comparison in the stratosphere with other profiles from satellite, balloon, aircraft, and ground-based data have shown an overall agreement of 5–10 % (Livesey et al., 2015). We use MLS version 4.2 ozone profile data for the comparison with ozonesonde data. Considering data quality metrics, we filter the qualified data based on the recommended process in Livesey et al. (2015). For selecting the reliable stratospheric region, we only use the pressure height range from 261.0 to 4.6 hPa.

2.2.3 OMPS limb profiler ozone profile

The Limb Profiler (LP) is a part of the OMPS instrument onboard the Suomi NPP satellite launched in October 2011. The OMPS LP provides a full global coverage per ~4 days, measuring scattered solar radiation in UV and VIS spectral ranges. Then ozone profiles are separately retrieved using wavelengths pairs in the UV range (OMPS UV algorithm: 302, 312, and 322 nm paired with 353 nm), and triplets in the VIS range (OMPS VIS algorithm: 600 nm combined with 510 and 675 nm to form a single VIS triplet). The OMPS VIS algorithm retrieves ozone in a lower altitude (~12.5 km) than the OMPS UV algorithm. To compare more massive amounts of ozone profiles with ozonesonde, we use data from the OMPS VIS algorithm (version 2.5) with a valid altitude range (12.5 to 33.5 km) and high quality flag

(Johnson 2017; Kramarova et al., 2018).

2.4 Equivalent latitude

To understand the spatial pattern of Antarctic ozone depletion, the influence of the polar vortex should be investigated. The Jang Bogo station is mostly located inside the polar vortex range but sometimes located outside, associated with the day-to-day variation of polar vortex size and strength. To consider this variation, we utilize the equivalent latitude (EqL), indicating where it has an equal effect of a polar vortex. In other words, the usage of the EqL enables us to find if the target site is under the polar vortex influence or not (Nash et al., 1996; Añel et al., 2013). Therefore, spatial criteria for the validation (i.e., coincidence criteria) is determined using the relative EqL difference between ozonesonde and satellite ozone data at the Jang Bogo station (description in detail in chapter 3). Since the EqL is calculated from the potential vorticity (PV), here we use PV data on the 475K potential temperature height where the atmospheric dynamic is dominantly controlled by Polar vortex (Kuttippurath et al., 2010; Gazeaux et al., 2013). PV values are obtained from the European Centre for Medium-Range Weather Forecasts reanalysis 5th Generation (ERA5) data for the latitude and longitude resolution of 0.25˚ by 0.25˚.

3. Comparison methodology

As mentioned above, previous studies used a range of coincidence criteria, implying the spatiotemporal situation required for the comparison between ozonesonde and satellite observation. Kroon et al. (2011) applied coincidence criteria of ± 0.5˚ for both latitude and longitude and ±12 hours. Huang et al. (2017) filtered all OMI pixels within ±1˚ latitude, ±3˚ longitude, and ±6 hours of each ozonesonde measurement at first, and finally selected the nearest OMI pixel within 100 km from the launching station. Kramarova et al. (2014) decided the coincidence if OMPS and MLS ozone profiles

with ozonesonde observations are within ± 1˚ latitude, and ± 4˚ longitude for an altitude range from 13.5 to 21.5 km. Compared to previous works, our coincidence criteria in this study are a little loose because we would use sufficient data for the validation as much as possible. Our approaches are described as a following; First, coincidence criteria are applied within ± 3˚ for latitude and ± 10˚ for longitude spatially, and within the temporal criterion ± 8 hours. Next, we examine if both ozonesonde and satellite ozone data are under a similar dynamical status or not, based on the calculated EqL at 475 K potential temperature levels. We decide to use the case for the validation if EqL values from both ozonesonde and satellite measurements are within ± 3˚, which was used in van Gijsel et al. (2010) to avoid the comparison between different air masses in the Antarctic region (i.e., air mass from the inside or outside of polar vortex). Figure 4 shows the colocation pattern of distance and time between ozonesonde and satellite measurement in this study. Limb-viewing satellites (MLS and OMPS) show the difference ~150 to 300 km spatially and ~4 to 6 hours temporally. Nadir-viewing satellites (OMI PROFOZ) shows relatively smaller difference < 100 km spatially and ~2 to 7 hours temporally.

For the comparison between the ozonesonde and satellite ozone profiles, we also need to consider the difference in vertical resolution. Since the satellite measurement has a lower resolution, the ozone mixing ratio at a given altitude does not reflect the compact variation on a small scale, which can be detected by the ozonesonde measurement. To reduce this impact of different vertical resolutions in the comparison process (so-called smoothing errors), the high-resolution (~ 100 m) ozonesonde profiles are smoothed into each satellite vertical resolution using the averaging kernel convolution approach, called as the convolution process that have been widely used for this kind of comparison (e.g., Bak et al., 2015). This convolution process is shown as the Equation (1) below.

$$X_{smooth} = X_{apriori} + AKs\ (X_{sonde} - X_{apriori}) \quad (1)$$

where X_{sonde} is the ozonesonde profile integrated into the satellite ozone profile grid, $X_{apriori}$ is the a priori ozone profile used in the retrieval of satellite ozone profile (X_{sat}), and AKs is the satellite

averaging kernel matrix. The smoothing ozonesonde profile (X_{smooth}) is a reconstruction of the ozonesonde profile to match with the vertical resolution and sensitivity of the satellite retrieval (Rodgers, 2000).

Each satellite measurement provides the $X_{apriori}$ used in its own ozone profile retrieval. The usage of $X_{apriori}$ in the convolution process is to avoid unrealistic statistics skewed by minimal values in the reference data (Liu et al., 2010). Once X_{smooth} obtained after the convolution process, finally we can evaluate the satellite ozone profile X_{sat}. The mean relative error between satellite and smoothing ozonesonde profile (MRE_{sat}) is frequently considered for the quantitative evaluation in addition to the absolute difference ($X_{sat} - X_{smooth}$). MRE_{sat} is calculated as shown in Equation (2).

$$\mathrm{MRE_{sat}}(\%) = \frac{1}{\mathrm{n}}\sum_{i=1}^{n}\left(\frac{X_{sat}-X_{smooth}}{X_{aprioiri}}\right) \times 100. \quad (2)$$

In addition to MRE_{sat}, MRE between a priori and smoothed ozone profile ($MRE_{apriori}$) is also used for the evaluation. $MRE_{apriori}$ enables us to assess the quality of a priori ozone profile for the ozone profile retrieval of each satellite. Similar to the Equation (2), $MRE_{apriori}$ is calculated as shown in Equation (3).

$$MRE_{apriori}(\%) = \frac{1}{n}\sum_{i=1}^{n}\left(\frac{X_{apriori}-X_{smooth}}{X_{apriori}}\right) \times 100. \quad (3)$$

4. Result and discussion

Figure 5 shows all used profiles of the ozone volume mixing ratio (VMR) and temperature from ozonesonde and satellite measurements used in the Jang Bogo station. For most of the year, the amount of ozone is generally about 5 ppmv in the ozone layer, but it drops rapidly below 1 ppmv during the austral spring (September to mid-October). It seems that satellite measurements tend to have higher ozone concentrations throughout the ozone layer. The minimum TOC from these measurements occurred on 19 October 2015, which was 160.1 DU. Under this ozone depletion condition, PV at 475K was remarkably lower than -45×10^{-6} $K\cdot m^2\cdot kg^{-1}\cdot s^{-1}$. Considering that the edge of polar vortex usually

reveals the PV values from −30 to -45×10^{-6} $K\cdot m^2\cdot kg^{-1}\cdot s^{-1}$ at 475K during the August to November (Kuttippurath et al., 2010), this minimum TOC looks associated with the strongest polar vortex in the whole period of this study.

At first, we focus on ozone profiles in this case (19 October 2015) showing the largest ozone depletion to see the capability of each satellite for detecting the Antarctic ozone hole. For each satellite data, we compare four different ozone profiles: ozone profile from the ozonesonde measurement, ozone profile from the satellite measurement, smoothing ozonesonde ozone profile based on the Equation (1), and a priori ozone profile used in each satellite retrieval algorithm (Fig. 6). Ozone depletion strongly occurs in the lower stratosphere (10 to 20 km), and ozonesonde detects ~0.2 ppmv here. While all satellite retrieval algorithms just consider a priori ozone profile not to have ozone depletion in the lower stratosphere, their final ozone profile products well detect the ozone depletion pattern from 10 to 20 km. The OMI PROFOZ ozone profile looks especially impressive in spite of poor signal to noise ratios of nadir-viewing measurements. The performance of each satellite ozone profile can be evaluated quantitatively using MRE_{sat} values. For example, MRE_{sat} is 20.1% with OMI PROFOZ data, 14.1% with MLS data, and 21.4% with OMPS data at ~18 km where the satellite ozone profile shows the largest depletion. But the ozonesonde profile shows the largest ozone depletion at ~ 13 km, resulted in much larger MRE_{sat} values. This case study implies that the satellite measurement can capture the in-situ (ozonesonde) ozone profile, but the quantitative difference is not consistent according to the altitude. This is the point that we need to remember when we need to use the satellite ozone profile related to the analysis for the connection between the stratospheric ozone variation and climate variability.

Comparison of averaging kernels (AKs) let us know which sensor has a high or low sensitivity to the atmospheric ozone because AKs indicate the contribution of information at each altitude. Comparison of the corresponding AKs among OMI PROFOZ, MLS, and OMPS on 19 October 2015 (Fig. 7) reveals that the ozone retrieval information mainly came from the measurements in the 15 km to 30 km. The peak AKs values of the MLS and OMPS (limb-viewing) are higher than the OMI

PROFOZ (nadir-viewing); The AKs of the MLS and OMPS are ~0.6-0.7, but those of the OMI PROFOZ satellite are < 0.5, indicating that limb viewing satellite can have better sensitivity to the stratospheric ozone variation. Instead, OMI PROFOZ has some AKs in the upper troposphere, which are not much found in the MLS and OMPS data; OMPS only has AKs in the stratosphere, in particular. For the research about the ozone profile near the tropopause, therefore the usage of nadir-viewing ozone profile can be considered in spite of relatively lower AKs.

For more general evaluation, we compare ozone profiles of OMI PROFOZ, OMPS, and MLS against ozonesonde ozone profiles for the longer period from 2015 to 2018. Still the austral spring (September to December) is the target period (related to the ozone hole occurrence). Figure 8 indicates the annual pattern of absolute mean difference between the satellite and smoothing ozonesonde profile ($X_{sat} - X_{smooth}$) for OMI PROFOZ, MLS, and OMPS data. While MLS and OMPS data show consistent pattern of $X_{sat} - X_{smooth}$, $X_{sat} - X_{smooth}$ of OMI PROFOZ data show a larger annual variation. Ozone profiles of OMI PROFOZ in 2016 and 2017 have larger absolute difference than those in 2015 and 2018, which can be demonstrated by the horizontal traveling distance of ozonesonde measurement as shown in Fig. 2. Ozonesonde measurements in September and October 2016 and 2017 illustrate longer zonal and meridional travels (Fig. 2), meaning that the nadir-viewing ozone profiles over a specific pixel area can have large deviation from the ozonesonde profiles collected from wider area. Different from the nadir-viewing satellite, limb-viewing measurements technically provide ozone profile over broader area, therefore annual variation is not much found with MLS and OMPS ozone profiles. Between MLS and OMPS, MLS measurements tend to show higher ozone than ozonesonde measurements in altitudes > 20 km; $X_{sat} - X_{smooth}$ can be ~1 ppm at maximum. This comparison means that the OMPS ozone profile relatively captures ozonesonde profile well. Nonetheless, 4-year mean pattern looks similar for all three satellite ozone profiles.

Since the ozone mixing ratio is much larger in the ozone layer staying > ~20 km, absolute mean difference can be larger naturally in the stratosphere. Thus, we also evaluate the satellite ozone profiles

using the relative difference value, which is the MRE_{sat} calculated from the Equation (2). As shown in Fig. 8, MRE_{sat} values are mostly in the range from about -20 to 30%. Although there is a large exception (MRE_{sat} of OMI PROFOZ is > 60% at 15 km), this relative difference looks not bad in general compared to previous works. For example, Huang et al. (2017), which used exactly same method for the MRE_{sat} calculation, showed MRE_{sat} from -30 to 20 % in the Antarctic region (60 to 90 °S). Quantitative comparison based on other previous references is not perfectly possible because of the different calculation of relative biases and the difference of target area and time period, but findings from other comparison studies between satellite and ozonesonde ozone profile in the Antarctic region also look similar to our results (Gazeaux et al., 2013, Sepúlveda et al., 2021). Consequently, this study about the comparison between satellite and ozonesonde ozone profile at the Jang Bogo station confirms that the quality of satellite ozone profiles is also valid in the eastern Antarctica where the validation with ozonesonde was rarely performed.

Several technical issues have been reported for the factors to induce the biases of satellite ozone profile: inherent reduction in retrieval sensitivity to lower altitudes at larger solar zenith angles as a result of reduced photon penetration into the atmosphere (Huang et al., 2017), unrealized retrieval sensitivity arising from interferences by surface albedo (Liu et al., 2010), or unexpected thermal sensitivity of the instrument (Kramarova et al., 2018). But the property of a priori ozone profile is usually considered to evaluate the quality of satellite ozone profiles. Thus, we also investigate the $MRE_{apriori}$ calculated from the Equation (3), which is the relative difference between a priori ozone profile used in the satellite ozone retrieval algorithm and smoothing ozonesonde profiles. As a result, we find that $MRE_{apriori}$ values of OMI PROFOZ data are in the range from about -30 to 30 %, while $MRE_{apriori}$ values of MLS and OMPS reach about -70 % at maximum (Fig. 10). This feature means that a priori ozone profile was well assumed in the OMI PROFOZ retrieval algorithm. We found above that the quality of OMI PROFOZ ozone profile is not the best but comparable to that of MLS and OMPS ozone profile. Considering the nadir-viewing ozone profile usually has less observation sensitivity as

shown by lower AKs (Fig. 7), the moderate performance of OMI PROFOZ ozone profile may be attributed to the high agreement of a priori ozone profile to the general pattern of Antarctic ozone profile. This feature is probably a coincidence, but well represents the importance of a priori information in the satellite ozone retrieval.

5. Summary and conclusion.

Using ozonesonde measurement at the Jang Bogo station, this study performed the validation of ozone profiles retrieved from the three satellite measurements that have been widely used: OMI, MLS, and OMPS. Since satellite ozone profile was rarely validated with in-situ ozone measurements in polar regions, the officially first usage of ozonesonde data at this site will be very informative to the scientists when they need to use satellite ozone dataset for the analysis of polar atmospheric environment and climate pattern. Also, a number of previous satellite ozone profiles were usually validated based on a single satellite product, evaluating the performance of multiple satellite ozone profile can provide the idea about the judicious usage of various satellite ozone products, particularly about the simultaneous consideration of ozone profiles from both nadir- and limb-viewing measurements.

As a result, we confirmed that all three satellite products moderately captures the stratospheric ozone profile from ozonesonde measurements in the Jang Bogo station, while satellite ozone profiles have a little higher value. Compared to the ozonesonde profile, satellite ozone profiles show absolutely ~1 ppm and relatively about -20 to 30 % at maximum, which is similar to the result of some previous studies. We also confirmed that a priori ozone information plays a significant role for the retrieval of qualified ozone profile from the satellite measurements. Although the nadir-viewing satellite generally has lower quality of ozone profile due to the lower AKs than the limb-viewing satellite technique, the quality of OMI PROFOZ ozone profile in this study looks comparable to MLS and OMPS ozone profiles in terms of long-term average pattern. Since the total ozone column from OMI measurements have been widely examined, it seems useful to use the OMI PROFOZ ozone profile if possible. Still the

usage of limb-viewing MLS or OMPS ozone profile can guarantee more accurate analyses (e.g., OMI PROFOZ has a large inter-annual variation as shown in Fig. 8), but our study can suggest the simultaneous usage of multiple satellite ozone profiles, enabling us to have more reliable average pattern, and more abundant data coverage (e.g., nadir-viewing satellites also provides the ozone profile in the troposphere).

Antarctic stratospheric ozone has been monitored for a long time in terms of the ozone hole events inducing the increase of dangerous ultraviolet radiation from the space. Fortunately, this issue has been resolved by the global efforts and now the Antarctic ozone shows the recovery signal (Solomon et al., 2016). But the importance of Antarctic ozone study is still valid. At this present moment, Antarctic ozone variation is considered to figure out the pattern of climate variability in the Antarctic area, and its influence to the regional environment (Son et al., 2009; Thompson et al., 2011). Owing to deficient measurements in the Antarctic area, however, the measurement-based analysis of ozone-climate connection was spatially limited much, ozone profiles in particular. Since stratosphere-troposphere exchange of ozone is a representative feature related to the ozone-climate connection (Thompson et al., 2011), the investigation of ozone profile should be more facilitated. We will more focus on the judicious usage of satellite ozone profile, which still includes some uncertainties, but becomes more qualified.

Acknowledgements.

This study was supported by the Korea Polar Research Institute (grant no. PE20070). This research was also supported by the Yonsei Signature Research Cluster Program of 2021 (2021-22-0003).

Data availability

The satellite ozone profiles Level-2 data, TOC Level-3 data, and PV reanalysis data used in this work were obtained from:

- OMI PROFOZ Level-2 version 1 (available at https://avdc.gsfc.nasa.gov/pub/data/satellite/Aura/OMI/V03/L2/OMPROFOZ/),
- OMPS Level-2 version 2.5 (available at https://snpp-omps.gesdisc.eosdis.nasa.gov/data/SNPP_OMPS_Level2/OMPS_NPP_LP_L2_O3_DAILY.2),
- MLS Level-2 version 4.2 (available at https://cmr.earthdata.nasa.gov/search/concepts/C1251101678-GES_DISC.html),
- ERA-5 PV (available at https://cds.climate.copernicus.eu/cdsapp#!/dataset/reanalysis-era5-single-levels?tab=form).

The ground-based ozonesonde and Brewer measurements in this contribution are available on google-drive (Contacting the first and corresponding authors are strongly recommended before pulling data from that google-drive).

Reference

Ahn, D.H., Choi, T., Kim, J., Park, S.S., Lee, Y.G., Kim, S.J., Koo, J.H., 2019: Southern Hemisphere mid- and high-latitudinal AOD, CO, NO_2, and HCHO: spatiotemporal patterns revealed by satellite observations. Prog. Earth Planet. Sci., 6, 34, https://doi.org/10.1186/s40645-019-0277-y.

Añel, J.A., Allen, D.R., Sáenz, G., Gimeno, L., de la Torre, L., 2013: Equivalent Latitude Computation Using Regions of Interest (ROI). PLoS One, 8, e72970, https://doi.org/10.1371/journal.pone.0072970.

Bais, A.F., Lucas, R.M., Bornman, J.F., Williamson, C.E., Sulzberger, B., Austin, A.T., Wilson, S.R., Andrady, A.L., Bernhard, G., McKenzie, R.L., Aucamp, P.J., Madronich, S., Neale, R.E., Yazar, S., Young, A.R., De Gruijl, F.R., Norval, M., Takizawa, Y., Barnes, P.W., Robson, T.M., Robinson, S.A., Ballaré, C.L., Flint, S.D., Neale, P.J., Hylander, S., Rose, K.C., Wängberg, S., Häder, D.P., Worrest, R.C., Zepp, R.G., Paul, N.D., Cory, R.M., Solomon, K.R., Longstreth, J., Pandey, K.K., Redhwi, H.H., Torikai, A., Heikkilä, A.M., 2018: Environmental effects of ozone depletion, UV

radiation and interactions with climate change: UNEP Environmental Effects Assessment Panel, update 2017. Photochem. Photobiol. Sci., 17, 127–179. https://doi.org/10.1039/c7pp90043k.

Bak, J., Liu, X., Kim, J.H., Chance, K., Haffner, D.P., 2015: Validation of OMI total ozone retrievals from the SAO ozone profile algorithm and three operational algorithms with Brewer measurements. Atmos. Chem. Phys., 15, 667–683, https://doi.org/10.5194/acp-15-667-2015.

Ball, W.T., Alsing, J., Mortlock, D.J., Staehelin, J., Haigh, J.D., Peter, T., Tummon, F., Stübi, R., Stenke, A., Anderson, J., Bourassa, A., Davis, S.M., Degenstein, D., Frith, S., Froidevaux, L., Roth, C., Sofieva, V., Wang, R., Wild, J., Yu, P., Ziemke, J.R., Rozanov, E. V., 2018: Evidence for a continuous decline in lower stratospheric ozone offsetting ozone layer recovery. Atmos. Chem. Phys., 18, 1379–1394, https://doi.org/10.5194/acp-18-1379-2018.

Ball, W.T., Alsing, J., Staehelin, J., Davis, S.M., Froidevaux, L., Peter, T., 2019: Stratospheric ozone trends for 1985-2018: Sensitivity to recent large variability. Atmos. Chem. Phys., 19, 12731–12748. https://doi.org/10.5194/acp-19-12731-2019.

Boylan, P., Wang, J., Cohn, S.A., Fetzer, E., Maddy, E.S., Wong, S., 2015: Validation of AIRS version 6 temperatureprofiles and surface-based inversionsover Antarctica using Concordiasidropsonde data, J. Geophys. Res. Atmos.,120, 992–1007.

Cionni, I., Eyring, V., Lamarque, J.F., Randel, W.J., Stevenson, D.S., Wu, F., Bodeker, G.E., Shepherd, T.G., Shindell, D.T., Waugh, D.W., 2011: Ozone database in support of CMIP5 simulations: Results and corresponding radiative forcing. Atmos. Chem. Phys., 11, 11267–11292, https://doi.org/10.5194/acp-11-11267-2011.

Farman, J.C., Gardiner, B.G., Shanklin, J.D., 1985: Large losses of total ozone in Antarctica reveal seasonal ClO x/NOx interaction. Nature, 315, 207-210, https://doi.org/10.1038/315207a0.

Gazeaux, J., Clerbaux, C., George, M., Hadji-Lazaro, J., Kuttippurath, J., Coheur, P.F., Hurtmans, D., Deshler, T., Kovilakam, M., Campbell, P., Guidard, V., Rabier, F., Thépaut, J.N., 2013: Intercomparison of polar ozone profiles by IASI/MetOp sounder with 2010 Concordiasi

ozonesonde observations. Atmos. Meas. Tech., 6, 613–620, https://doi.org/10.5194/amt-6-613-2013.

Goutail, F., Hauchecorne, A., Pazmiño, A., Quel, E., Khaykin, S., Claud, C., Wolfram, E., Godin-Beekmann, S., Salvador, J., 2018: Multiple symptoms of total ozone recovery inside the Antarctic vortex during austral spring. Atmos. Chem. Phys., 18, 7557–7572, https://doi.org/10.5194/acp-18-7557-2018,

Huang, G., Liu, X., Chance, K., Yang, K., Bhartia, P.K., and co-authors, 2017: Validation of 10-year SAO OMI Ozone Profile (PROFOZ) product using ozonesonde observations. Atmos. Meas. Tech., 10, 2455-2475, https://doi.org/10.5194/amt-10-2455-2017.

Huang, G., Liu, X., Chance, K., Yang, K., Cai, Z., 2018: Validation of 10-year SAO OMI Ozone Profile (PROFOZ) Product Using Aura MLS Measurements. Atmos. Meas. Tech., 11, 17-32, https://doi.org/10.5194/amt-11-17-2018.

Ivy, D.J., Solomon, S., Kinnison, D., Mills, M.J., Schmidt, A., Neely, R.R., 2017: The influence of the Calbuco eruption on the 2015 Antarctic ozone hole in a fully coupled chemistry-climate model. Geophys. Res. Lett., 44, 2556–2561, https://doi.org/10.1002/2016GL071925

Johnson, J., 2017: README Document for Suomi-NPP OMPS NPBUVO3-L2 Product.

Kim, S., Park, S.-J., Lee, H., Ahn, D.H., Jung, Y., Choi, T., Lee, B.Y., Kim, S., and Koo, J.-H., 2021: Evaluation of total ozone column from multiple satellite measurements in the Antarctic using the Brewer spectrophotometer, Remote Sens., 13, 1594.

Komhyr, W.D., Air Resources Laboratory (U.S.), 1986: Operations handbook--ozone measurements to 40-km altitude with model 4A electrochemical concentration cell (ECC) ozonesondes (used with 1680-MHz radiosondes), NOAA technical memorandum ERL ARL.

Koo, J.H., Choi, T., Lee, H., Kim, Jaemin, Ahn, D.H., Kim, Jhoon, Kim, Y.H., Yoo, C., Hong, H., Moon, K.J., Lee, Y.G., 2018: Total ozone characteristics associated with regional meteorology in West Antarctica. Atmos. Environ.. 195, 78–88, https://doi.org/10.1016/j.atmosenv.2018.09.056.

Kramarova, N.A., Nash, E.R., Newman, P.A., Bhartia, P.K., McPeters, R.D., Rault, D.F., Seftor, C.J., Xu, P.Q., Labow, G.J., 2014: Measuring the Antarctic ozone hole with the new ozone mapping and profiler suite (OMPS). Atmos. Chem. Phys., 14, 2353–2361, https://doi.org/10.5194/acp-14-2353-2014.

Kramarova, N.A., Bhartia, P.K., Jaross, G., Moy, L., Xu, P., Chen, Z., Deland, M., Froidevaux, L., Livesey, N., Degenstein, D., Bourassa, A., Walker, K.A., Sheese, P., 2018: Validation of ozone profile retrievals derived from the OMPS LP version 2.5 algorithm against correlative satellite measurements. Atmos. Meas. Tech., 11, 2837–2861, https://doi.org/10.5194/amt-11-2837-2018.

Kroon, M., De Haan, J.F., Veefkind, J.P., Froidevaux, L., Wang, R., Kivi, R., Hakkarainen, J.J., 2011: Validation of operational ozone profiles from the Ozone Monitoring Instrument. J. Geophys. Res., 116, D18305, https://doi.org/10.1029/2010JD015100.

Kuttippurath, J., Godin-Beekmann, S., Lefèvre, F., Santee, M.L., Froidevaux, L., Hauchecorne, A., 2015: Variability in Antarctic ozone loss in the last decade (2004-2013): High-resolution simulations compared to Aura MLS observations. Atmos. Chem. Phys., 15, 10385–10397, https://doi.org/10.5194/acp-15-10385-2015.

Kuttippurath, J., Goutail, F., Pommereau, J.P., Lefévre, F., Roscoe, H.K., Pazmĩno, A., Feng, W., Chipperfield, M.P., Godin-Beekmann, S., 2010: Estimation of Antarctic ozone loss from ground-based total column measurements. Atmos. Chem. Phys., 10, 6569–6581, https://doi.org/10.5194/acp-10-6569-2010.

Kuttippurath, J., Lefèvre, F., Roscoe, H.K., Goutail, F., Pazmiño, A., Shanklin, J.D., 2013: Antarctic ozone loss in 1979-2010: First sign of ozone recovery. Atmos. Chem. Phys., 13, 1625-1635, https://doi.org/10.5194/acp-13-1625-2013.

Kuttippurath, J., Nair, P.J., 2017: The signs of Antarctic ozone hole recovery. Sci. Rep., 7, 585, https://doi.org/10.1038/s41598-017-00722-7.

Levelt, P.F., Van Den Oord, G.H.J., Dobber, M.R., Mälkki, A., Visser, H., De Vries, J., Stammes, P., Lundell, J.O.V., Saari, H., 2006: The ozone monitoring instrument. IEEE Trans. Geosci. Remote Sens., 44, 1093-1101, https://doi.org/10.1109/TGRS.2006.872333.

Liu, X., Bhartia, P.K., Chance, K., Spurr, R.J.D., Kurosu, T.P., 2010: Ozone profile retrievals from the Ozone Monitoring Instrument. Atmos. Chem. Phys., 10, 2521–2537, https://doi.org/10.5194/acp-10-2521-2010.

Liu, X., Chance, K., Sioris, C.E., Spurr, R.J.D., Kurosu, T.P., Martin, R. V., Newchurch, M.J., 2005: Ozone profile and tropospheric ozone retrievals from the Global Ozone Monitoring Experiment: Algorithm description and validation. J. Geophys. Res., 110, 1–19, https://doi.org/10.1029/2005JD006240.

Liu, X., Bhartia, P.K., Chance, K., Froidevaux, L., Spurr, R.J.D., Kurosu, T.P., 2010: Validation of Ozone Monitoring Instrument (OMI) ozone profiles and stratospheric ozone columns with Microwave Limb Sounder (MLS) measurements. Atmos. Chem. Phys., 10, 2539-2549, https://doi.org/10.5194/acp-10-2539-2010.

Livesey, N. J., Read, W. G., Wagner, P. A., Froidevaux, L., Lambert, A., Manney, G. L., Millan Valle, L.F., Pumphrey, H. C., Santee, M. L., Schwartz, M. J., Wang, S., Fuller, R. A, Jarnot, R. F., Knosp, B. W., and Martinez, E., 2015: Earth Observing System (EOS), Aura Microwave Limb Sounder (MLS) 169.

Livesey, N.J., Filipiak, M.J., Froidevaux, L., Read, W.G., Lambert, A., Santee, M.L., Jiang, J.H., Pumphrey, H.C., Waters, J.W., Cofield, R.E., Cuddy, D.T., Daffer, W.H., Drouin, B.J., Fuller, R.A., Jarnot, R.F., Jiang, Y.B., Knosp, B.W., Li, Q.B., Perun, V.S., Schwartz, M.J., Snyder, W. V., Stek, P.C., Thurstans, R.P., Wagner, P.A., Avery, M., Browell, E. V., Cammas, J.-P., Christensen, L.E., Diskin, G.S., Gao, R.-S., Jost, H.-J., Loewenstein, M., Lopez, J.D., Nedelec, P., Osterman, G.B., Sachse, G.W., Webster, C.R., 2008: Validation of Aura Microwave Limb Sounder O_3 and CO

observations in the upper troposphere and lower stratosphere. J. Geophys. Res., 113, D15S02, https://doi.org/10.1029/2007jd008805.

Manney, G.L., Lawrence, Z.D., 2016: The major stratospheric final warming in 2016: Dispersal of vortex air and termination of Arctic chemical ozone loss. Atmos. Chem. Phys., 16, 15371–15396, https://doi.org/10.5194/acp-16-15371-2016.

Mateer, C.L., Deluisi, J.J., 1992: A new Umkehr inversion algorithm. J. Atmos. Terr. Phys., 54, 537-556, https://doi.org/10.1016/0021-9169(92)90095-3.

McPeters, R.D., Labow, G.J., Logan, J.A., 2007: Ozone climatological profiles for satellite retrieval algorithms. J. Geophys. Res., 112, D05308, https://doi.org/10.1029/2005JD006823.

Miyagawa, K., Petropavlovskikh, I., Evans, R.D., Long, C., Wild, J., Manney, G.L., Daffer, W.H., 2014: Long-term changes in the upper stratospheric ozone at Syowa, Antarctica. Atmos. Chem. Phys., 14, 3945-3968, https://doi.org/10.5194/acp-14-3945-2014.

Nash, E.R., 1996: An objective determination of the polar vortex using Ertel's potential vorticity. J. Geophys. Res., 101, 9471–9478, https://doi.org/10.1029/96JD00066.

Nassar, R., Logan, J.A., Worden, H.M., Megretskaia, I.A., Bowman, K.W., Osterman, G.B., Thompson, A.M., Tarasick, D.W., Austin, S., Claude, H., Dubey, M.K., Hocking, W.K., Johnson, B.J., Joseph, E., Merrill, J., Morris, G.A., Newchurch, M., Oltmans, S.J., Posny, F., Schmidlin, F.J., Vömel, H., Whiteman, D.N., Witte, J.C., 2008: Validation of Tropospheric Emission Spectrometer (TES) nadir ozone profiles using ozonesonde measurements. J. Geophys. Res. Atmos., 113, 1–13, https://doi.org/10.1029/2007JD008819.

Newton, R., Vaughan, G., Ricketts, H.M.A., Pan, L.L., Weinheimer, A.J., Chemel, C., 2016: Ozonesonde profiles from the West Pacific Warm Pool: Measurements and validation. Atmos. Chem. Phys., 16, 619–634, https://doi.org/10.5194/acp-16-619-2016.

Oss, V., n.d. Ozone profile algorithm, in: OMI Algorithm Theoretical Basis Document, Vol- ume II: OMI ozone products. 2001.

Rabier, F., Cohn, S., Cocquerez, P., Hertzog, A., Avallone, L., Deshler, T., Haase, J., Hock, T., Doerenbecher, A., Wang, J., Guidard, V., Thépaut, J.N., Langland, R., Tangborn, A., Balsamo, G., Brun, E., Parsons, D., Bordereau, J., Cardinali, C., Danis, F., Escarnot, J.P., Fourrié, N., Gelaro, R., Genthon, C., Ide, K., Kalnajs, L., Martin, C., Meunier, L.F., Nicot, J.M., Perttula, T., Potts, N., Ragazzo, P., Richardson, D., Sosa-Sesma, S., Vargas, A., 2013: The concordiasi field experiment over antarctica: First results from innovative atmospheric measurements. Bull. Am. Meteorol. Soc., 94, 17–20, https://doi.org/10.1175/BAMS-D-12-00005.1.

Rault, D.F., Loughman, R.P., 2013: The OMPS limb profiler environmental data record algorithm theoretical basis document and expected performance. IEEE Trans. Geosci. Remote Sens., 51, 2505-2527, https://doi.org/10.1109/TGRS.2012.2213093.

Rodgers, C.D., 2000: 00 INVERSE METHODS FOR ATMOSPHERIC SOUNDING Theory and Practice, World Scientific Publishing Co.Pte.Ltd.

Sepúlveda, E., Cordero, R.R., Damiani, A., Feron, S., Pizarro, J., Zamorano, F., Kivi, R., Sánchez, R., Yela, M., Jumelet, J., Godoy, A., Carrasco, J., Crespo, J.S., Seckmeyer, G., Jorquera, J.A., Carrera, J.M., Valdevenito, B., Cabrera, S., redondas, A., and Rowe, R.M., 2021: Evaluation of Antarctic Ozone Profiles derived from OMPS-LP by using Balloon-borne Ozonesondes, Sci. Rep., 11, 4288, https://doi.org/10.1038/s41598-021-81954-6.

Sheshadri, A., Alan Plumb, R., Domeisen, D.I.V., 2014: Can the delay in antarctic polar vortex breakup explain recent trends in surface westerlies? J. Atmos. Sci., 71, 566–573, https://doi.org/10.1175/JAS-D-12-0343.1.

Solomon, S., Ivy, D.J., Kinnison, D., Mills, M.J., Neely III, R.R., Schmidt, A., 2016: Emergence of healing in the Antarctic ozone layer. Science, 353, 269–274. https://doi.org/10.1126/science.aae0061.

Son, S.-W., Tandon, N.F., Polvani, L.M., Waugh, D.W., 2009: Ozone hole and southern hemisphere climate change. Geophys. Res. Lett., 36, L15705.

Sounding, O., Rs, V.R., n.d. USER ' S GUIDE Ozone Sounding with Vaisala Radiosonde.

Steinbrecht, W., Froidevaux, L., Fuller, R., Wang, R., Anderson, J., Roth, C., Bourassa, A., Degenstein, D., Damadeo, R., Zawodny, J., Frith, S., McPeters, R., Bhartia, P., Wild, J., Long, C., Davis, S., Rosenlof, K., Sofieva, V., Walker, K., Rahpoe, N., Rozanov, A., Weber, M., Laeng, A., von Clarmann, T., Stiller, G., Kramarova, N., Godin-Beekmann, S., Leblanc, T., Querel, R., Swart, D., Boyd, I., Hocke, K., Kämpfer, N., Maillard Barras, E., Moreira, L., Nedoluha, G., Vigouroux, C., Blumenstock, T., Schneider, M., Garcìa, O., Jones, N., Mahieu, E., Smale, D., Kotkamp, M., Robinson, J., Petropavlovskikh, I., Harris, N., Hassler, B., Hubert, D., Tummon, F., 2017: An update on ozone profile trends for the period 2000 to 2016. Atmos. Chem. Phys., 17, 10675-10690, https://doi.org/10.5194/acp-17-10675-2017

Thompson, A.M., Miller, S.K., Tilmes, S., Kollonige, D.W., Witte, J.C., Oltmans, S.J., Johnson, B.J., Fujiwara, M., Schmidlin, F.J., Coetzee, G.J.R., Komala, N., Maata, M., Bt Mohamad, M., Nguyo, J., Mutai, C., Ogino, S.Y., Da Silva, F.R., Leme, N.M.P., Posny, F., Scheele, R., Selkirk, H.B., Shiotani, M., Stbi, R., Levrat, G., Calpini, B., Thouret, V., Tsuruta, H., Canossa, J.V., Vmel, H., Yonemura, S., Diaz, J.A., Tan Thanh, N.T., Thuy Ha, H.T., 2012: Southern Hemisphere Additional Ozonesondes (SHADOZ) ozone climatology (2005-2009): Tropospheric and tropical tropopause layer (TTL) profiles with comparisons to OMI-based ozone products. J. Geophys. Res., 117, D23301, https://doi.org/10.1029/2011JD016911.

Thompson, A.M., Witte, J.C., McPeters, R.D., Oltmans, S.J., Schmidlin, F.J., Logan, J.A., Fujiwara, M., Kirchhoff, V.W.J.H., Posny, F., Coetzee, G.J.R., Hoegger, B., Kawakami, S., Ogawa, T., Johnson, B.J., Vömel, H., Labow, G., 2003: Southern Hemisphere Additional Ozonesondes (SHADOZ) 1998-2000 tropical ozone climatology 1. Comparison with Total Ozone Mapping Spectrometer (TOMS) and ground-based measurements. J. Geophys. Res., 108, 8238, https://doi.org/10.1029/2001jd000967.

Thompson, A.M., Witte, J.C., Smit, H.G.J., Oltmans, S.J., Johnson, B.J., Kirchhoff, V.W.J.H., Schmidlin, F.J., 2007: Southern Hemisphere Additional Ozonesondes (SHADOZ) 1998-2004 tropical ozone climatology: 3. Instrumentation, station-to-station variability, and evaluation with simulated flight profiles. J. Geophys. Res., 112, D03304, https://doi.org/10.1029/2005JD007042.

Thompson, D.W.J., Solomon, S., Kushner, P.J., England, M.H., Grise, K.M., Karoly, D.J., 2011: Signatures of the Antarctic ozone hole in Southern Hemisphere surface climate change. Nat. Geosci., 4, 741–749.

Van Gijsel, J.A.E., Swart, D.P.J., Baray, J.L., Bencherif, H., Claude, H., Fehr, T., Godin-Beekmann, S., Hansen, G.H., Keckhut, P., Leblanc, T., McDermid, I.S., Meijer, Y.J., Nakane, H., Quel, E.J., Stebel, K., Steinbrecht, W., Strawbridge, K.B., Tatarov, B.I., Wolfram, E.A., 2010: GOMOS ozone profile validation using ground-based and balloon sonde measurements. Atmos. Chem. Phys., 10, 10473–10488. https://doi.org/10.5194/acp-10-10473-2010.

Wang, L., Newchurch, M.J., Biazar, A., Liu, X., Kuang, S., Khan, M., Chance, K., 2011: Evaluating AURA/OMI ozone profiles using ozonesonde data and EPA surface measurements for August 2006. Atmos. Environ., 45, 5523–5530, https://doi.org/10.1016/j.atmosenv.2011.06.012.

Yoo, J.H., Choi, T., Chun, H.Y., Kim, Y.H., Song, I.S., Song, B.G., 2018: Inertia-Gravity Waves Revealed in Radiosonde Data at Jang Bogo Station, Antarctica (74°37′S, 164°13′E): 1. Characteristics, Energy, and Momentum Flux. J. Geophys. Res. Atmos., 123, 13305-13331, https://doi.org/10.1029/2018JD029164.

Zuev, V. V., Savelieva, E., 2019: The cause of the spring strengthening of the Antarctic polar vortex. Dyn. Atmos. Ocean., 87, 101097, https://doi.org/10.1016/j.dynatmoce.2019.101097.

Table 1. Specification of satellite ozone profile data used in this paper.

Instrument		**OMI**	**MLS**	**OMPS LP**
Principle		Nadir-viewing backscatter	Limb-viewing thermal emission	Limb-viewing backscatter
Satellite		Aura	Aura	Suomi-NPP
Product name		PROFOZ	ML2O3	OMPS-NPP LP
Wavelengths used in the ozone retrieval		270-330 nm	240 GHz	600 nm combined with 510 nm and 675 nm (VIS)
Algorithm version		version 3.0[1] version 0.9.3[2]	version 4.2[3]	version 2.5[4]
Ozone a priori		McPeters et al. (2007)	MOZART model-based climatology	McPeters and Labow (2014)
Altitude valid range		Surface-65 km	261.0-0.02 hPa	12.5-33.5 km
Spatial resolution (along track × across track)		13 km × 48 km (at nadir)	165 km x 3 km	125 km x 2 km
Horizontal coverage		1 day	15 orbits per day	14.5 orbits per day
Vertical resolution		2 - 3 km	3 - 6 km	1.8 km
Reference		Liu et al., (2010)	Livesey et al., (2015)	Kramarova et al., (2018)

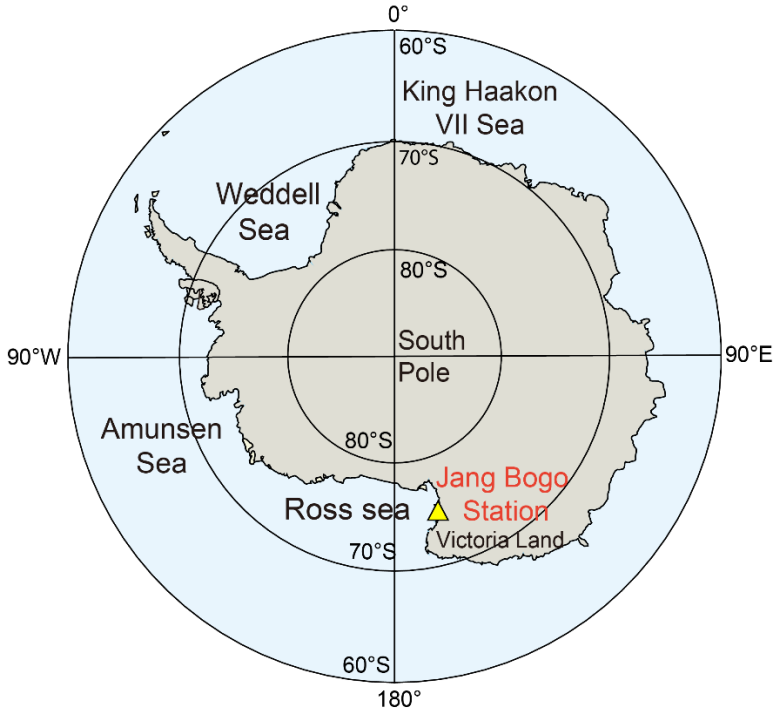

Figure 1. Map of Antarctica. The yellow triangle indicates the geographical locations of the Jang Bogo station.

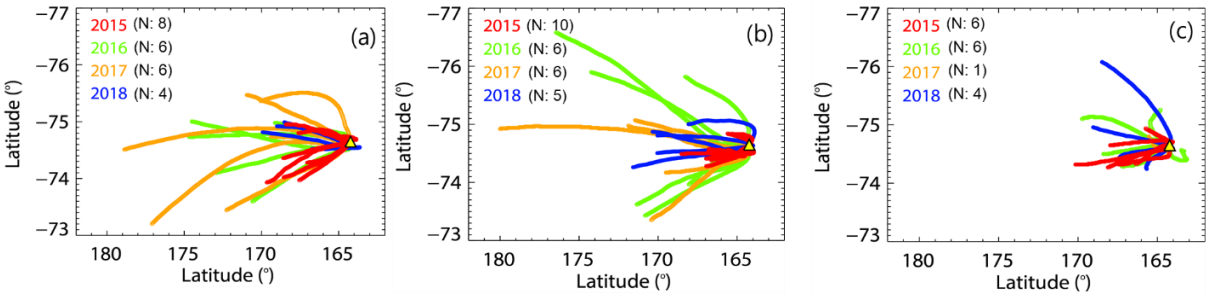

Figure 2. Trajectories of the all ozonesonde observations in (a) September, (b) October, and (c) November of the year 2015 (red), 2016 (green), 2017 (orange), and 2018 (blue). N indicates the total measurement number for each period.

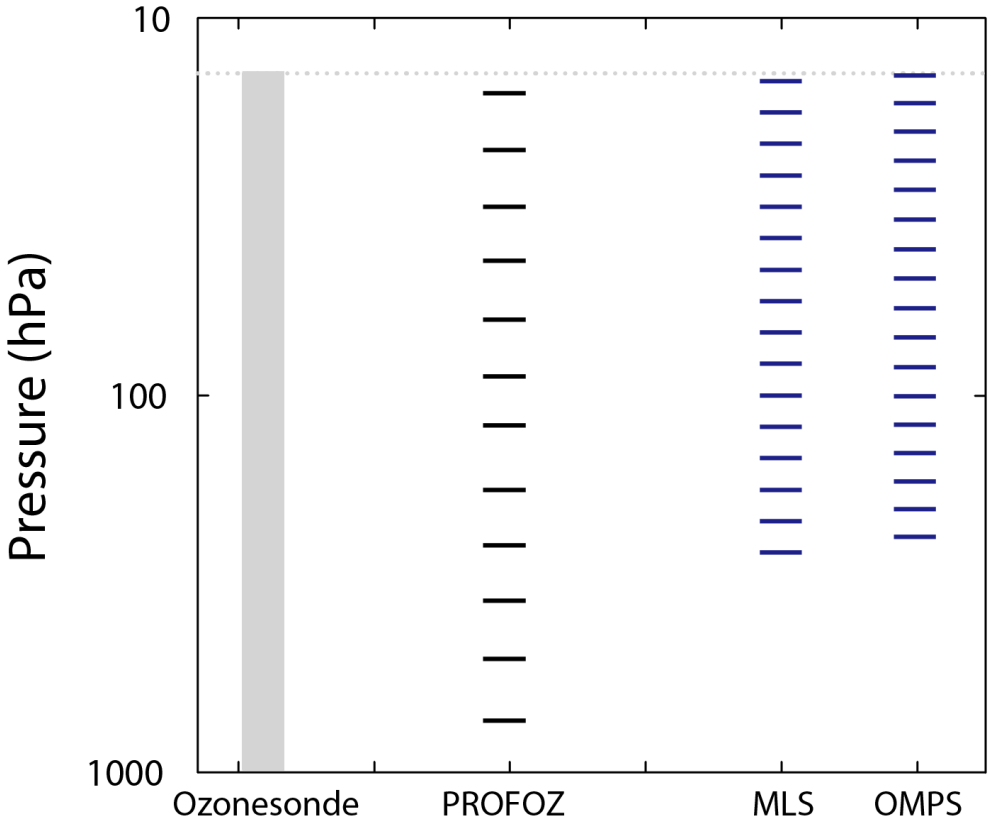

Figure 3. The vertical coverage and levels of ozone profiles from the ozonesonde (gray), nadir-viewing OMI PROFOZ (black), and limb-viewings MLS and OMPS (blue) measurements.

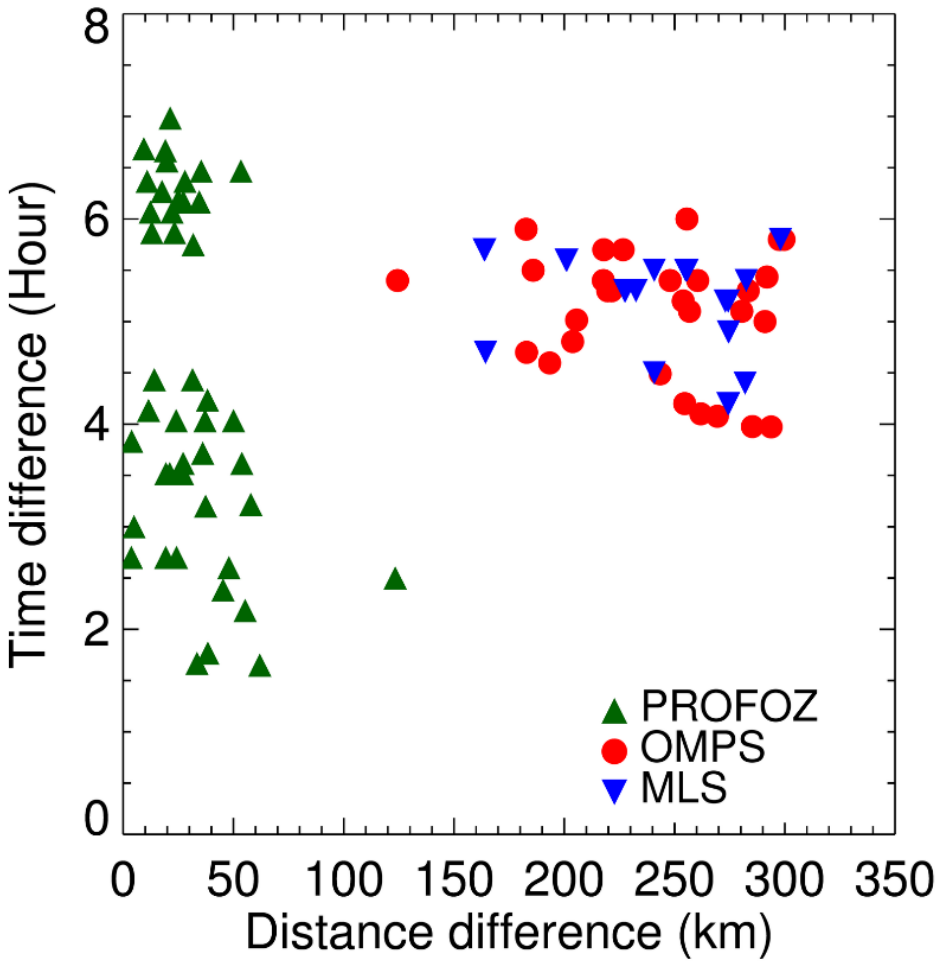

Figure 4. Difference of time (unit: hour) and horizontal distance (unit: km) between ozonesonde measurements at the Jang Bogo station and ozone measurement of OMI PROFOZ (green), OMPS (red), and MLS (blue) satellites.

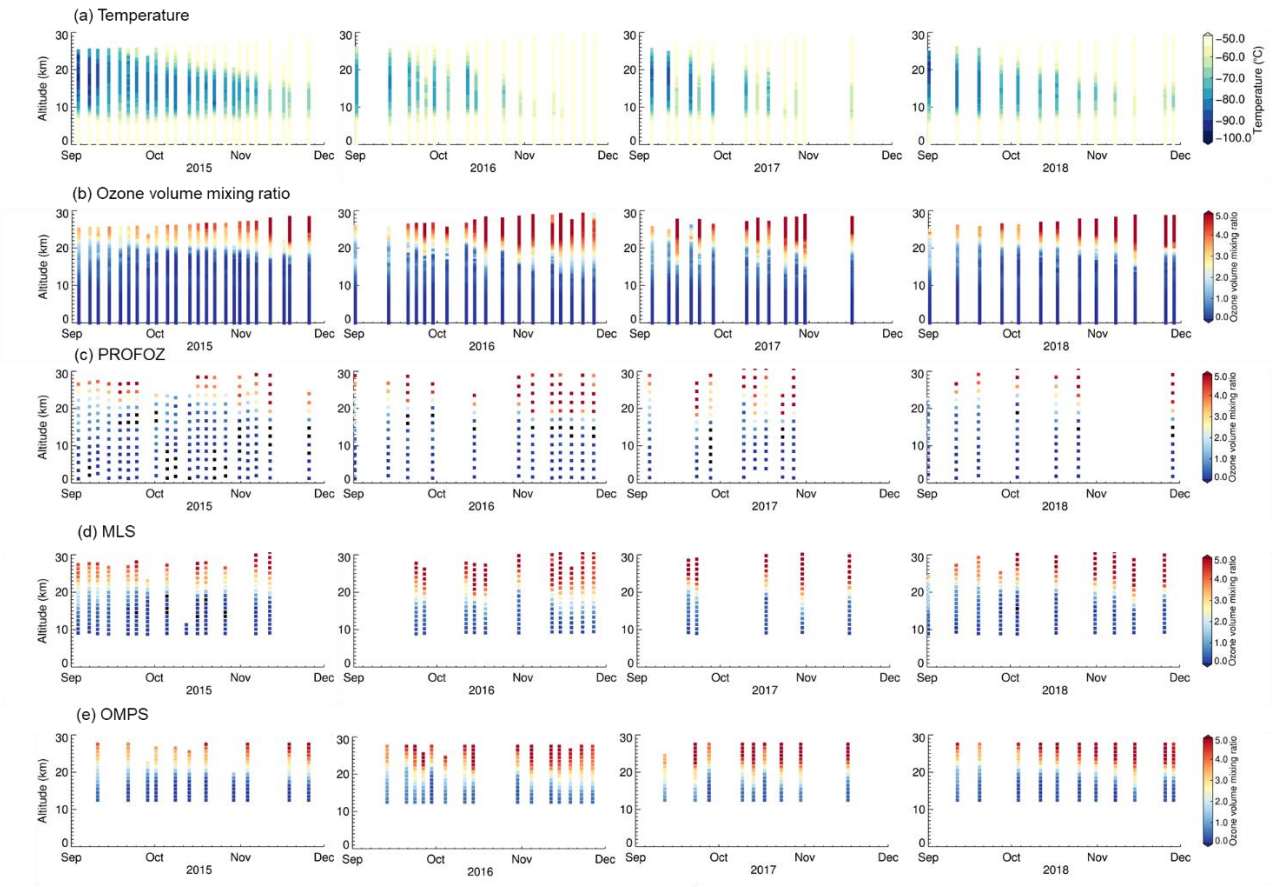

Figure 5. All vertical profiles of (a) temperature (b) ozone mixing ratio from ozonesonde measurements, compared with vertical ozone profiles of (c) OMI PROFOZ, (d) MLS, and (e) OMPS satellite measurements at the same time. The range of each value follows each color bar scale.

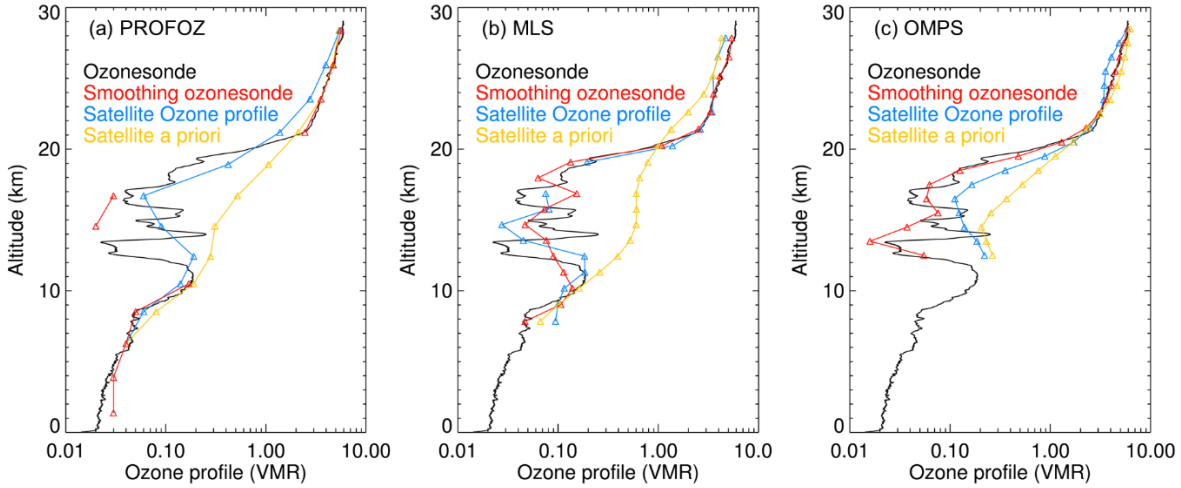

Figure 6. Comparisons among original ozonesonde profiles (black), smoothing ozonesonde profiles (red), satellite ozone profile (blue), and a priori ozone profiles used in satellite retrieval algorithm (yellow) on 19 October 2015, using three satellite data: (a) the OMI PROFOZ, (b) MLS, and (c) OMPS.

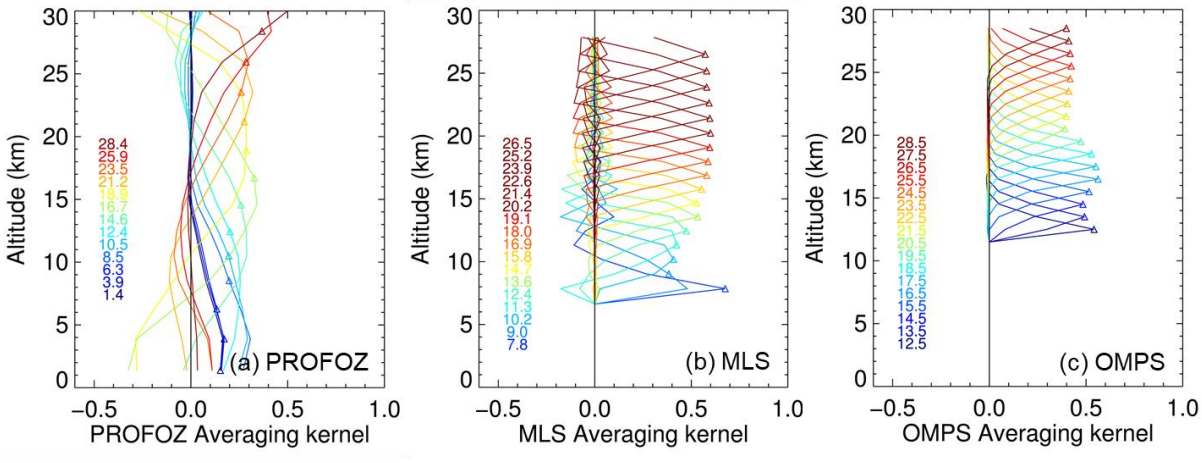

Figure 7. An example showing averaging kernels (AKs) of ozone profile from (a) OMI PROFOZ, (b) MLS, and (c) OMPS data on 19 October 2015 over the JBS. Each colored line indicates the altitude of retrieved ozone profile product (unit: km).

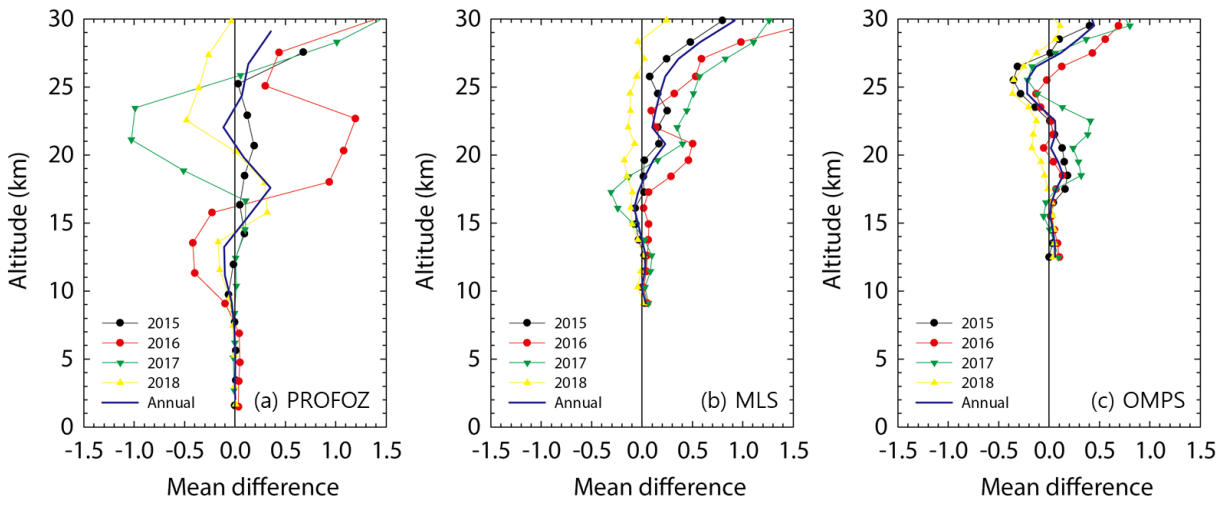

Figure 8. Absolute mean difference (X_{sat}- X_{smooth}) between ozonesonde and satellite ozone profile from (a) OMI PROFOZ, (b) MLS, and (c) OMPS data in 2015 (black), 2016 (red), 2017 (green), and 2018 (yellow). Total mean patterns are also depicted (blue).

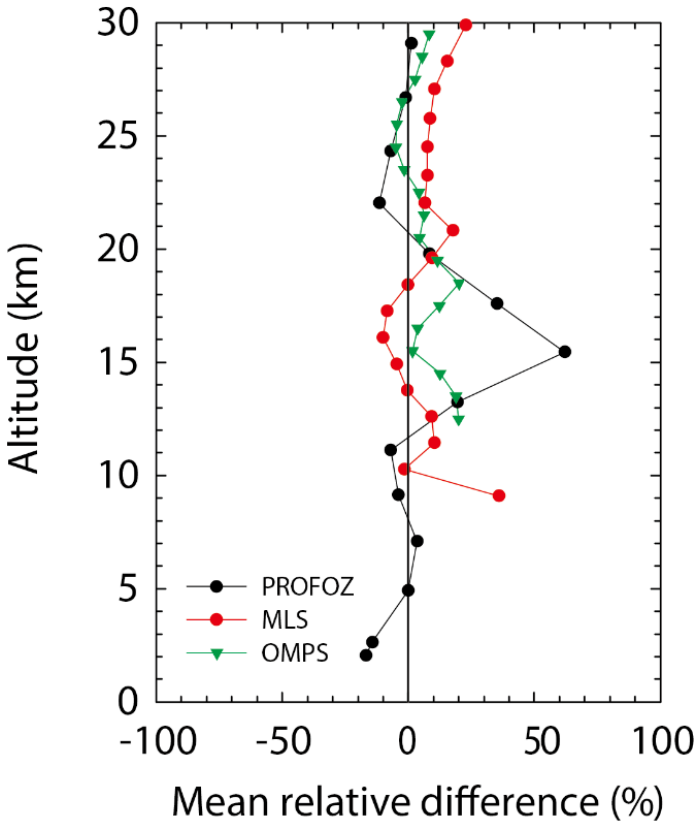

Figure 9. Vertical profile of 4-year mean MRE_{sat} values using the Equation (2) for OMI PROFOZ (black), MLS (red), and OMPS (green) data.

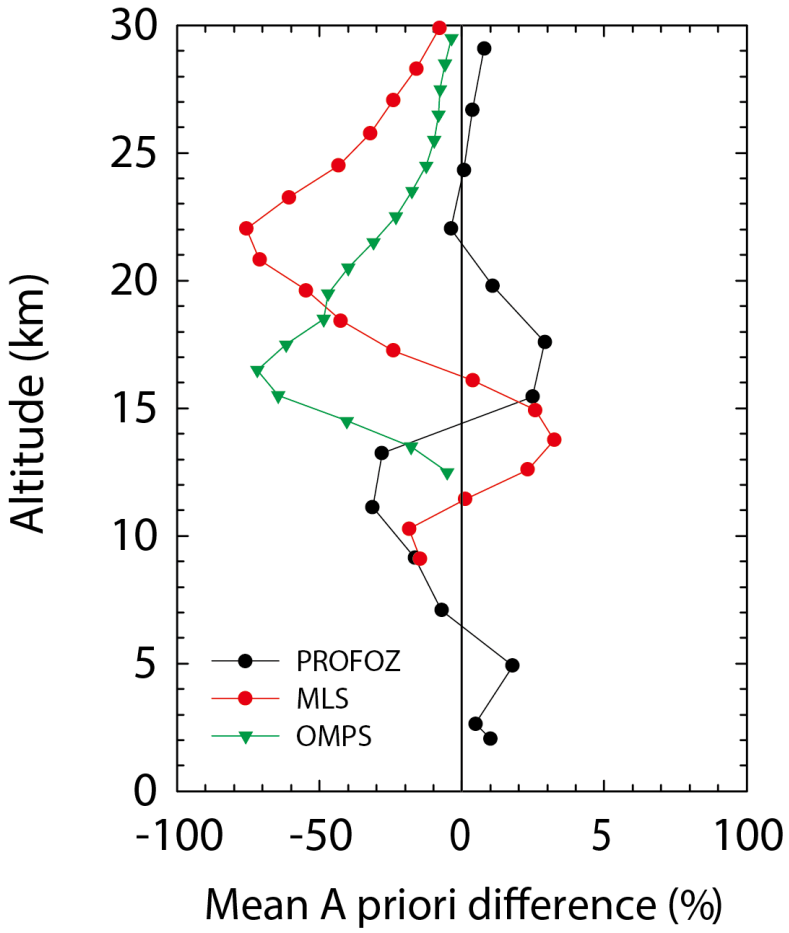

Figure 10. Vertical profile of 4-year mean $MRE_{apriori}$ values using the Equation (2) for OMI PROFOZ (black), MLS (red), and OMPS (green) data.